ELSEVIER

Biophysical Chemistry 85 (2000) 229–248

Biophysical Chemistry

www.elsevier.nl/locate/bpc

Bacteriorhodopsin: the functional details of a molecular machine are being resolved

Joachim Heberle, Jörg Fitter, Hans Jürgen Sass, Georg Büldt*

Forschungszentrum Jülich, IBI-2: Structural Biology, D-52425 Jülich, Germany

Abstract

The photon-driven proton translocator bacteriorhodopsin is considered to be the best understood membrane protein so far. It is nowadays regarded as a model system for photosynthesis, ion pumps and seven transmembrane receptors. The profound knowledge came from the applicability of a variety of modern biophysical techniques which have often been further developed with research on bacteriorhodopsin and have delivered major contributions also to other areas. Most prominent examples are electron crystallography, solid-state NMR spectroscopy and time-resolved vibrational spectroscopy. The recently introduced method of crystallising a membrane protein in the lipidic cubic phase led to high-resolution structures of ground state bacteriorhodopsin and some of the photocycle intermediates. This achievement in combination with spectroscopic results will strongly advance our understanding of the functional mechanism of bacteriorhodopsin on the atomic level. We present here the current knowledge on specific aspects of the structural and functional dynamics of the photoreaction of bacteriorhodopsin with a focus on techniques established in our institute.

Keywords: Retinal protein; Proton transfer; X-Ray crystallography; Neutron scattering; FT-IR spectroscopy

1. The photochemical reaction

Almost 30 years ago, bacteriorhodopsin (bR) was found in *Haloarchea* [1] and represents a simple photosynthetic machinery that uses light energy to translocate protons out of the cell interior [2]. Photon absorption by the chromophore *all-trans* retinal, covalently bound to K216 of the apoprotein to form a protonated azomethine (Schiff base), initiates a series of colour changes [3]. Finally, bacteriorhodopsin relaxes back to the ground state where it can be restarted [4–6]. The photocycle intermediates are detectable by visible spectroscopy (see [7] for a comprehensive review). Fig. 1 displays the photocycle with the nomencla-

* Corresponding author. Tel.: +49-2461-61-2030; fax: +49-2461-61-2020.

E-mail address: g.bueldt@fz–juelich.de (G. Büldt).

0301-4622/00/$ - see front matter
PII: S0301-4622(99)00154-4

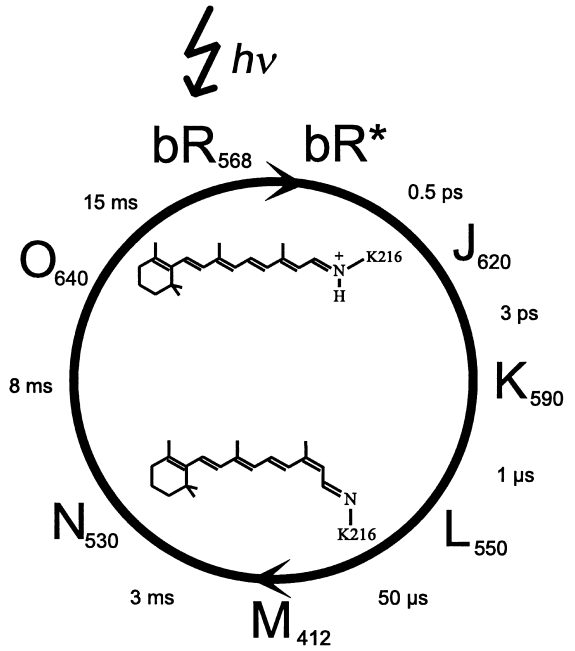

Fig. 1. The photocycle of bR showing the light-adapted ground state bR_{568}, the excited state (bR*) and the intermediates (J, K, L, M, N, and O) with their absorption maxima and lifetimes. The lifetimes have been determined at neutral pH and 20°C. The conformations of *all-trans* and 13-*cis* retinal are also depicted.

ture of the intermediates. They are characterised by their absorption maximum and their lifetimes spanning the enormous range of 11 decades.

Excitation of the bR ground state leads to the formation of a sub-picosecond product, termed the J intermediate [8,9]. The transition of the vibrationally hot J intermediate [10] to the subsequent K state proceeds with a time constant of 3 ps [8]. The appearance of hydrogen-out-of-plane vibrations indicated a distorted 13-*cis* configuration of retinal [11,12]. Relaxation of this configurational strain leads via the KL intermediate to the L intermediate [13–15]. Thus, the initial photo-induced *trans/cis* isomerisation of retinal is finally settled in the L intermediate.

The subsequent M intermediate represents the key intermediate of the photocycle as the retinal Schiff base (RSB) has lost the proton [16]. This results in a dramatic blue shift of the absorbance spectrum whereas the spectra of all of the other intermediates strongly overlap with ground-state bR. The spectral overlap together with the kinetic complexity of the photocycle conversions impeded the elucidation of the detailed kinetic scheme of the photoreactions of bR. Deprotonation of the Schiff base initiates a series of proton transfer reactions within the protein that finally leads to proton translocation across the whole membrane. The late intermediates, N and O, are characterised by a reprotonated RSB. The colour difference between these intermediates might be ascribed to the different retinal configuration which is 13-*cis* in N and *all-trans* in the O state.

The photocycle kinetics strongly depends on pH which is not surprising for a proton pump. In particular, the lifetimes of the late intermediates are drastically changed by pH variation. Acidic pH promotes the transient accumulation of the O intermediate whereas in the alkaline the N state dominates the latest stage of the photocycle. The transient concentration of L is decreased at elevated pH leading to an apparent faster rise of the M intermediate. These pH-dependent changes of the properties of bR are due to protonation changes of internal groups. It is obvious that the various pH-equilibria complicate a thorough analysis of the kinetics.

Most of the intermediates, as defined by their colour, have been subdivided for mechanistic reasons corroborated by spectroscopic and kinetic results. The transition of M_1 to M_2 is of primary interest since it comprises the switch, the prerequisite for vectorial catalysis. The switch is defined as the change in accessibility of the retinal Schiff base from the extracellular to the cytoplasmic side.

The transitions of the photocycle intermediates are thermally activated. For this reason, intermediate states can be trapped at low temperatures allowing detailed investigations in cases where sufficient time-resolution is lacking. The J intermediate, however, cannot be trapped at cryogenic temperatures. This fact served as an objection towards the existence of an early intermediate prior to the K state.

For a detailed understanding of the mechanism of proton translocation, methods are required that allow to trace the functional dynamics of bR

with high resolution both in time and space. An arsenal of methodologies have already been applied to bR. We will present in the following some of the results and their implications for the pumping mechanism of bR based on biophysical methods established in our institute.

2. The ground state structure of bR

2.1. The electron microscopic structure and the refinement by neutron and X-ray diffraction

The characterisation of the aggregation state of bR in the purple membrane was given by X-ray diffraction on these natural two-dimensional lattices [17,18]. The basic picture of the tertiary structure, describing the three-dimensional arrangement of α-helices spanning the membrane, was published in several papers on low-dose electron microscopy [19,20]. The knowledge of the amino acid sequence [21] allowed the prediction of a folding model by determining seven α-helical stretches in the polypeptide chain, which were assigned to the seven α-helices seen in the electron microscopical structure [22]. In the following years neutron diffraction was the method of choice to prove this model using bR molecules containing certain perdeuterated amino acids [23,24] and partially deuterated α-helices [25,26]. This technique was also successful in the localisation of perdeuterated or partially deuterated retinal within the protein [27–29]. Heavy-atom labelled retinal analogues incorporated into the protein confirmed these results by X-ray diffraction [30]. The location of the proton channel in the low-resolution structure of bR was determined by neutron diffraction in combination with H_2O/D_2O exchange experiments [31].

In 1990, cryo-electron microscopy provided an additional breakthrough providing a structure of bR at 3.5 Å resolution in the *X–Y* plane and 7 Å in the *Z*-direction. This picture allowed for the first time, including all the information from other methods mentioned above, to construct a molecular model of bR [32]. This model was further improved by cryo-electron microscopy data of Grigorieff et al. [33], Kimura et al. [34] and Mitsuoka et al. [35].

2.2. Crystallisation of bR

bR was one of the first integral membrane proteins that was crystallised in three dimensions [36]. A considerable progress was obtained by using the surfaces of freshly formed benzamidine crystals as nucleation sites [37]. These plate-shaped crystals diffracted to 3.6 Å in the a and b direction and 4.2 Å in the c direction.

A novel concept for crystallisation of membrane proteins in a lipidic cubic phase has been reported by Landau and Rosenbusch [38]. They crystallised bR in a monoolein water cubic phase and obtained microcrystals of space group $P6_3$ with a unit cell of $a = b = 61.76$ Å; $c = 104.16$ Å, $\alpha = \beta = 90°$ and $\gamma = 120°$. Initially, very small microcrystals of up to 30 μm in diameter and 5 μm in thickness were grown. The crystallisation conditions were continuously improved so that crystals of 150 μm in diameter are available now. The cell constant in the a,b-direction of 61.76 Å together with the hexagonal space group gave an indication for an arrangement of bR molecules similar to the purple membrane. In accordance with the screw axis along the c direction these purple membrane like 2D lattices are stacked on each other, where two adjacent lattices are rotated by 60° [39]. Using a highly focused beam with a diameter of approximately the same size as the crystal, the signal-to-noise ratio was strongly increased, so that diffraction patterns of up to 2 Å resolution could be obtained.

2.3. Vibrational spectroscopy to assess the functionality of bR microcrystals

After solving the problem of crystallising a membrane protein the proper functionality of the protein within the crystal lattice has to be proven. Common tests on functionality of membrane proteins usually call for compartmentation. This strategy is apparently impossible with crystals. Thus, we employed vibrational spectroscopy as a non-invasive tool to assess the functionality of bR microcrystals.

The light-induced Fourier-transform infrared (FT-IR) difference spectrum of bR in the 3D crystal lattice is identical to that obtained with bR embedded in the natural purple membrane (see [40] for the experimental data). The resonance-Raman spectrum of a single microcrystal shows bands typical for bR in the ground state with an admixture of bands characteristic of the M intermediate due to the high laser intensity of the Raman experiment. Moreover, the millisecond kinetics of bR in the 3D crystal tally with those obtained in the natural 2D arrays of the purple membrane. Taken together, these results demonstrate that bR is fully functional in the 3D crystals. Since these results provide critical evidence that structural changes and proton translocation are not impaired by the crystallisation in lipidic cubic phase, the high resolution structure of bacteriorhodopsin discussed in the next section, represents the biologically active form in the 3D-crystals.

2.4. The crystal structure of the ground state of bR

The crystal structure of bR was solved by molecular replacement on the basis of the electron microscopic structure [33] to 2.5 Å resolution [39]. After improving the crystallisation conditions, larger crystals became available showing a high degree of merohedral twinning which had to be corrected for [41,42]. Meanwhile two additional crystal structures of bR were published resulting from different crystallisation strategies [43,44]. The structure of Essen et al. [43] nicely shows structural features of how lipids in the protein boundary interact with amino acid side chains. The most important new features of all of these structures are that the conformations of functionally important amino acid side chains become more and more reliable and that the location of several water molecules could be determined in the proton translocation pathway. Fig. 2 shows functionally important amino acids of the bR crystal structure from the light-adapted ground state, crystallised also from the lipidic cubic phase in our laboratory (for details see protein data bank entry 1cwq and [45]). The extracellular part of the molecule (below the retinal) exhibits a hydrogen-bonded network of charged amino acids and water molecules which are elements of the proton translocation pathway. However, without a comparison of the relevant intermediate structures (L, M, N) it is not possible to extract a unique mechanism for the proton translocation from this part of the structure. The different conformations of amino acid side chains and the positions of water molecules in these intermediates will allow to calculate pK-values of functionally important groups. Thus, it will be possible to explain the vectoriality of the process in this part of the molecule.

Very few charged amino acids and water molecules are located in the cytoplasmic domain of the molecule. It is still difficult to trace a probable proton translocation pathway in this part of the structure because there are mostly hydrophobic amino acids. For reprotonation of the Schiff base from the protein donor D96 a gap of approximately 11 Å has to be bridged.

3. Structure of intermediate states

3.1. Characterisation of intermediate states by infrared spectroscopy

Since more than 15 years vibrational spectroscopy (in particular resonance Raman scattering [46,47] and infrared absorption) added molecular information to the understanding of the proton pump. However, strong overlap of the $3N-6$ vibrations (with N = number of atoms) renders impossible to record highly resolved infrared absorption spectra of large proteins. A powerful technique to overcome this obstacle is difference spectroscopy where only those vibrations are selected that change during the action of the protein [48]. With the advent of Fourier-transform infrared (FT-IR) spectroscopy this procedure allows to record single vibrations in front of the whole protein. Even dynamics of single vibrations can be followed with high temporal resolution. Nanosecond difference spectra over a broad spectral range have been obtained by state-of-the-art FT-techniques [49–51].

Infrared spectroscopy was particularly helpful

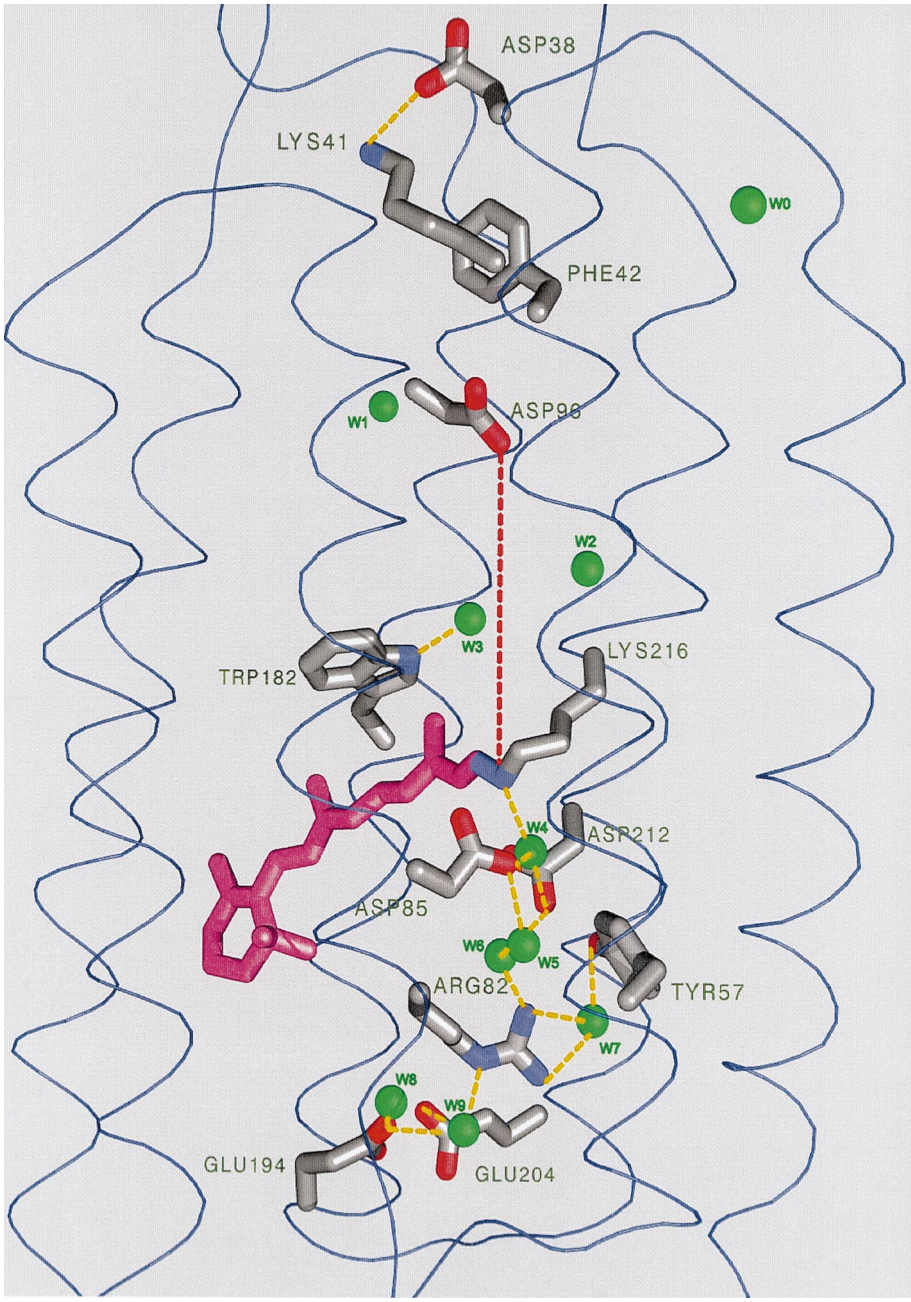

Fig. 2. Ground-state structure of bR with the cytoplasmic side up and the extracellular side down. The protein backbone is represented by thin ribbons (blue). Several functionally important residues and water molecules (W0–W9 in green) are shown. *All-trans* retinal is in purple colour. Broken yellow lines indicate hydrogen bonding distances ranging from 2.3 to 3.4 Å. The broken red line which is approximately 11 Å long, depicts the distance from D96 to the retinal Schiff base. Structural coordinates have been deposited on the protein data bank (entry: 1cwq).

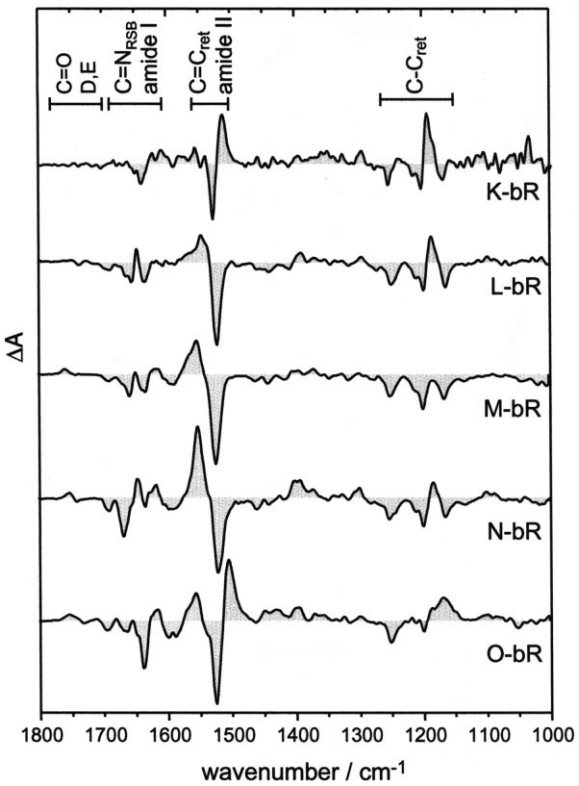

Fig. 3. Infrared difference spectra of the photocycle intermediates of bR. All but the K-bR spectrum have been extracted from time-resolved ATR/FT-IR experiments under the following conditions: L-bR (10 μs, pH 6.6, 20°C), M-bR (300–400 μs, pH 8.4, 20°C), N-bR (80–100 ms, pH 8.4, 20°C), and O-bR (5–10 ms, pH 4.0, 40°C). The K-bR difference spectrum was obtained under steady-state conditions (continuous illumination of a bR microcrystal with $\lambda = 514$ nm from an argon ion laser, sample is kept at 100 K). Spectra are scaled to yield identical negative absorbance at 1252 cm^{-1}. Regions of marker bands are indicated by horizontal bars (D = aspartic acid; E = glutamic acid; RSB = retinal Schiff base; ret = Retinal).

in elucidating the role of particular amino acids in proton translocation across bR [52–56]. Besides the detection of vibrational changes of the chromophore retinal as well as of the protein backbone, it is a major advantage of FT-IR spectroscopy that the protonation state of acidic amino acids can be observed. Step-scan spectroscopy allows to follow these transient changes with high temporal resolution [49,50,57].

Fig. 3 displays difference spectra between ground-state bR (negative bands) and the intermediates K, L, M, N, and O (positive bands). The range selected from 1800 to 1000 cm^{-1} is particularly useful because of the richness in band features. Except for the K-bR spectrum, the displayed difference spectra have been obtained with time-resolved attenuated total reflection (ATR) FT-IR spectroscopy. This evanescent wave technique where the sample is immersed in excess water, allows for the precise control of parameters like pH, temperature and ionic strength [57,58]. Conditions have been chosen that maximise the transient concentration of the respective intermediate state (see figure caption and [59]).

The strongest band in Fig. 3 is located at 1526 cm^{-1} and has been assigned to the C=C double bond of retinal in the unphotolysed state (see [54] for a compilation of the band assignment). The corresponding bands of the photoproducts are shifted to 1512 cm^{-1} in K, 1549 cm^{-1} in L, 1555 cm^{-1} in M, 1553 cm^{-1} in N, and 1506 cm^{-1} in O. The C–C single bonds of the chromophore are absorbing in the region between 1150 and 1280 cm^{-1}. This spectral region is a marker region for the configuration of retinal. Appearance of the band around 1190 cm^{-1} reflects the *trans–cis* isomerisation at the $C_{13}=C_{14}$ bond. It is located at 1193 cm^{-1} in K, 1190 cm^{-1} in L, and 1184 cm^{-1} in N. This vibration can hardly be detected in the M intermediate because the dipole moment of retinal is much lower when the retinal Schiff base is deprotonated. The isomerisation state of retinal was thought to be *all-trans* during the lifetime of the O intermediate [60]. The appearance of large difference bands in the fingerprint region of the O-bR spectrum might argue for a *cis*-retinal. This hypothesis needs to be rigorously tested, however, by isotopic labelling of retinal.

The negative band at 1639 cm^{-1} has been attributed to the protonated Schiff base in the unphotolysed state of bR [16]. It is of equal intensity in L and M, much smaller in N and most pronounced in O. Other bands involving the Schiff base vibration can be found at 1302 cm^{-1} (C–H in-plane bending vibration) and 1400 cm^{-1} (N–H in-plane). Typical for the 13-*cis* chromophore, they are strong in L and N. Conformational

changes of the protein backbone are observable between 1500 and 1600 cm^{-1} (C=N–H, amide II) and between 1600 and 1700 cm^{-1} (C=O, amide I). They already show up in L and M, reach maximum intensity in N and are reversed in O. Bands above 1700 cm^{-1} are due to the C=O stretching vibration of protonated carboxylic acids coupled with the in-plane bending vibration of the O–H. These vibrational bands are indicative for the proton transfer reactions across bR and will be discussed in detail in Section 4.1.

In conclusion, infrared spectroscopy is capable to monitor the dynamics of retinal isomerisation, proton transfer as well as structural changes of the protein backbone in one experiment. Determination of the protonation state of single residues by crystallographic methods is very difficult. In this respect, IR spectroscopy is superior as it also delivers the temporal evolution of the proton transfer reactions.

3.2. X-Ray structure of the M intermediate

For a complete understanding of the function of a protein like bR it is desirable to follow-up structural changes in space and time with high resolution parallel to the working cycle. Since the intensity scattered from a single molecule is too low, taking into account the limits set by radiation damage, an ensemble of molecules has always to be considered. In this situation information about structural changes during the working cycle can be obtained in two ways, either by trapping intermediate states or by time-resolved detection of the scattered intensity after excitation. Both alternatives were successfully carried out in the case of bR.

3.2.1. Trapping of the M state

After the observation that a proton is translocated by bR to the extracellular side during the transition from L to M, the M intermediate was considered to be a strategic state for the pumping process. It seemed that knowledge of the M state structure would give some insight into the mechanism of proton translocation. One of the first trapping experiments of the M intermediate at low temperatures was performed by Glaeser et al. [61] using electron diffraction for detecting the M state structure. These experiments showed no intensity changes in the resolution region from 60 to 5 Å and small changes between 5 and 3.5 Å. Therefore, neutron diffraction experiments were undertaken by Dencher et al. [62] with the aim to observe changes in the distribution of water molecules in comparison to the ground state. As it was known that GuaHCl at high pH slows down the decay of the M state, a stack of several purple membrane (PM) films were soaked in a buffer containing GuaHCl at pH 9.4 and illuminated at +8°C. The films became yellow indicating the complete transformation to the M state, which was then preserved at liquid nitrogen temperatures in a cryostat. Neutron diffraction patterns of the ground state and of the M intermediate showed clear differences in the reflection intensities of up to 9% in $\Sigma|\Delta I|/\Sigma I$ in the resolution region of 60 to 7 Å. By comparing diffraction patterns between films in H_2O and D_2O it was derived that at least 80% of the differences resulted from changes in the protein structure and only a minor contribution could originate from a redistribution of water molecules. These observations indicate that small changes in the tertiary structure of bR take place during the photocycle. These results are in contradiction to the electron diffraction experiments of Glaeser et al. [61].

It was observed by optical spectroscopy that the bR mutant D96N is characterised by a large decrease in the decay rate of the M state with increasing pH. Koch et al. [63] performed X-ray diffraction experiments on films of this mutant under continuous illumination at room temperature and pH 9.6. They found similar changes between the bR_{568} and M_{412} state structures (Fig. 4B, 100% relative humidity, r.h.) as observed in the neutron diffraction measurements mentioned above.

3.2.2. Time-resolved X-ray diffraction experiment on the bR mutant D96N

In order to examine how these structural changes correlate with relaxation processes in the photo- and pumping cycle of bR, the structural transition from the M state to the ground state was followed by time-resolved X-ray diffraction

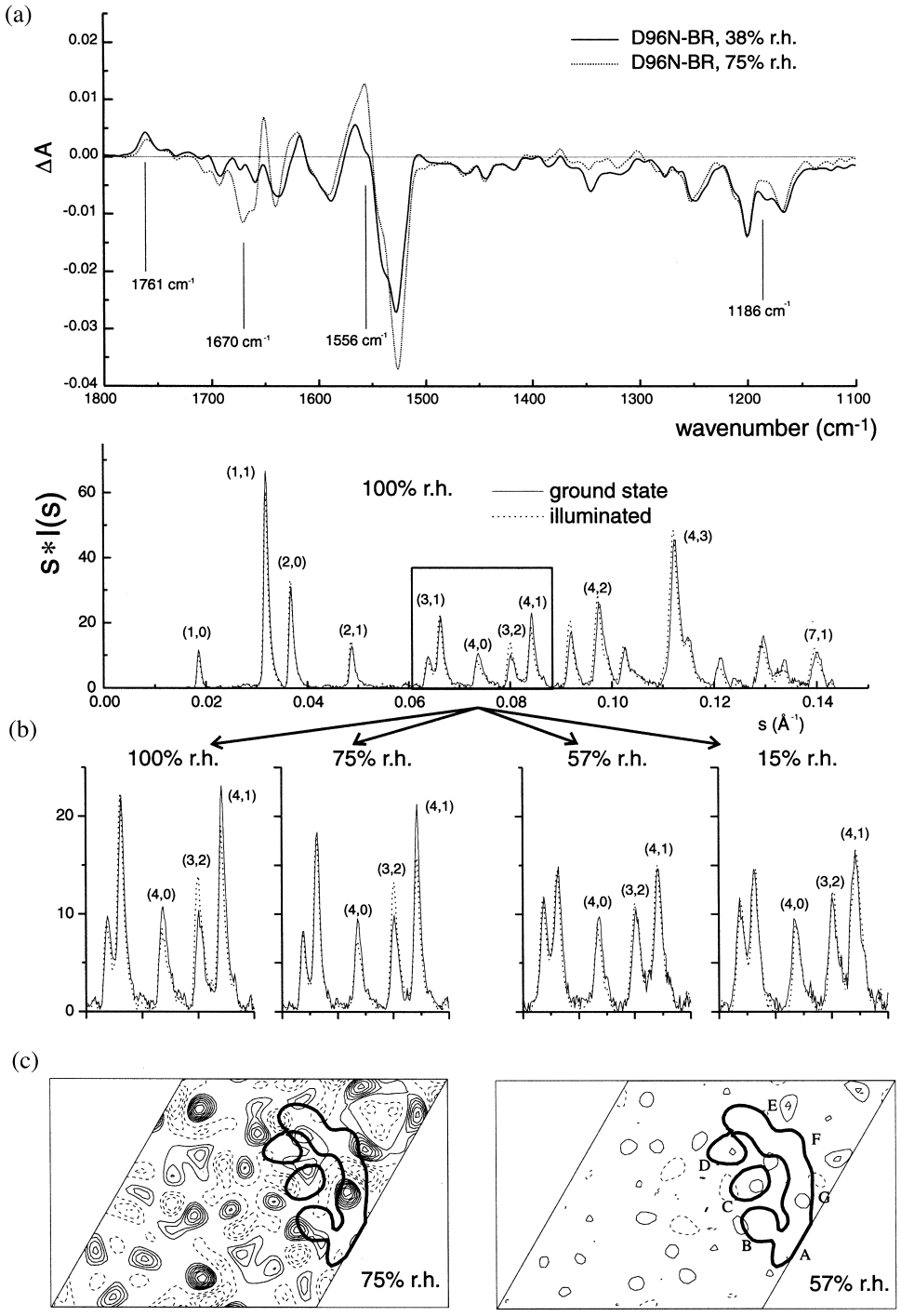
(a)
D96N-BR, 38% r.h.
D96N-BR, 75% r.h.
ΔA
1761 cm-1
1670 cm-1
1556 cm-1
1186 cm-1
wavenumber (cm-1)
100% r.h.
ground state
illuminated
S*I(S)
(1,1)
(2,0)
(1,0)
(2,1)
(3,1)
(4,0)
(3,2)
(4,1)
(4,2)
(4,3)
(7,1)
s (Å-1)
(b)
100% r.h.
75% r.h.
57% r.h.
15% r.h.
(c)
75% r.h.
57% r.h.
A
B
C
D
E
F
G

Fig. 4.

using intense synchrotron radiation [63]. The changes in individual reflections before and immediately after the light flash are consistent both in amplitude and in direction with the steady-state experiments.

A comparison of these structural relaxation times with optical decay rates of intermediate states in the photocycle indicated that the observed structural changes decay with the transition from the N state to the ground state. In functional terms this means that the structural changes relax after the reprotonation of the Schiff's base.

3.2.3. M splits into two states, M_1 and M_2

So far, only the relaxation of tertiary structural changes was followed by time-resolved X-ray experiments. The onset of these changes could not precisely be attributed to photocycle intermediates. A first hint for an answer to this problem was obtained from X-ray diffraction experiments on bR mutant D96N (pH 9.6) at different hydration levels [64]. PM films equilibrated at different relative humidities (15, 57, 75 and 100% r.h.) were transformed to the M state by continuous illumination. Films equilibrated at relative humidities above 60% showed the known changes in the tertiary structure, whereas films below 60% r.h. displayed only very small changes in their diffraction pictures (Fig. 4B). The corresponding difference density maps show positive difference density at helices B, F and G (Fig. 4C) at high humidity. No significant difference peaks can be seen below 60% r.h. These experiments demonstrated that two types of M states with and without structural changes compared to the ground state are existing. If one assumes that both M states would occur in the photocycle also at high hydration but in a sequential order, the changes in the tertiary structure would develop within the M intermediate between M_1 and M_2 and would relax after the N state. Reconsidering the earlier experiments of Glaeser et al. [61] it seems now very probable that the M_1 intermediate was accumulated and therefore no changes in the tertiary structure were observed.

FT-IR measurements under identical conditions, although with much thinner PM films, verify that for all hydration levels the films were trapped in the M intermediate. The distinction between the M and L intermediate as well as the N intermediate was made upon the finger print region of the FT-IR difference spectra, the most obvious criteria for such a differentiation (Fig. 4A). The largest differences between the differently hydrated samples were found in the amide regions. It appears that samples at hydration levels greater than 60% r.h. display the structural changes in the diffraction experiment and at the same time show in the amide I region a larger difference band at 1670 cm^{-1} than at 1660 cm^{-1} (M_2). On the other hand, the samples which do not show the changes in the tertiary structure (r.h. less than 60%) display a larger difference band at 1660 cm^{-1} than at 1670 cm^{-1} (M_1). These differences in the amide I region are also found in the amide II region, where the difference band at 1556 cm^{-1} is much larger in the more hydrated samples.

The concept of two M states was brought up from the evaluation of time-resolved spectroscopic data in the visible wavelength region [65]. An irreversible step was assumed at this position of the photocycle between M_1 and M_2 acting as a switch by changing the proton accessibility of the Schiff base from the extracellular to the cytoplasmic side and thus creating the vectoriality of the proton pump.

Fig. 4 (A) FT-IR difference spectra of bR-mutant D96N at 38% and 75% relative humidity (r.h.). (B) X-ray diffraction patterns of bR-D96N light-adapted purple membranes (pH 9.6, room temperature) at different hydration levels in the absence of light (solid line) and under steady-state illumination (dotted line). $s = 2\sin\theta/\lambda$, with Bragg angle θ and wavelength $\lambda = 1.5$ Å. The lower panels represent the reflection range (2,2) to (4,1) at different r.h. on an expanded scale. (C) Difference electron density maps (M state minus light-adapted ground state) of the bR-D96N purple membranes at different hydration levels. Left: 75% r.h., M_2 state. Right: 57% r.h., M_1 state. The bold contour outlines the bR monomer, individual helices are marked by upper case letters from A to G. Continuous lines correspond to positive, dashed lines to negative electron density levels. Contour levels are scaled to each other in both maps.

With respect to the function of bR, Thiedemann et al. [66] were able to show that proton pumping was only found in samples with hydration levels above 60% r.h. These results indicate that the observed structural changes are necessary for proton translocation and that at least part of these changes may form the switch which changes the accessibility to the Schiff's base.

3.2.4. Charge-controlled conformational changes

Further support for this interpretation of the proton translocation mechanism was given by the investigation of the bR mutant D38R [67]. X-Ray diffraction experiments on samples at pH 6.7 do not show changes in the tertiary structure of bR whereas measurements at pH 9.6 display a diffraction pattern, characteristic for structural changes. The interpretation of these experiments is, that at pH 6.7 the M_1-state is trapped under illumination whereas at pH 9.6 the M_2-state is accumulated. Assuming a sequential sequence of M_1 and M_2 independent of pH, it seems that also for this mutant the observed large structural changes are necessary for vectorial proton pumping. In addition, these results give a clear indication that the changes in the tertiary structure are driven by alterations in the charge distribution of the protein, which follow photoisomerisation.

The substitution of an aspartic acid by an arginine makes the charge pattern at the cytoplasmic side more positive either directly by the positive charge of the arginine or indirectly but more effectively since another positive charge is no longer compensated by the interaction with the aspartic acid. This new charge pattern, more positive at the cytoplasmic side than in wild-type bR, could interfere with the charge variation resulting from the deprotonation of the Schiff base and therefore slow down the large structural rearrangements. This would result in the accumulation of the M_1 state. Since no large structural changes are detectable under this condition and if one assumes a sequential order of M_1 and M_2 the general conclusion for wild-type bR can be drawn that a charge redistribution around the Schiff base and at the extracellular side of the molecule results in an altered force field within bR which drives the large structural changes. At a pH above 9, another group on the cytoplasmic side might be deprotonated and compensate at least partly the added positive charge of the arginine. This would allow the structural changes associated with the transition to the M_2 state to take place.

3.2.5. The M state structure at high resolution

Due to the new concept for crystallisation of bR in the lipidic cubic phase high resolution intermediate structures become available. Recently, Edman et al. [68] succeeded in solving the crystal structure of the early K intermediate and small structural changes with respect to the ground-state bR could be resolved. Luecke at al. [69] trapped the M state in crystals of the mutant D96N (PDB entries: 1c8r and 1c8s) which has a prolonged decay of the M state. The advantage of this mutant is that a high amount of M can be trapped at room temperature. The disadvantage is that, as indicated by the long decay time of M, the cytoplasmic proton translocation pathway is disturbed. Therefore, we have trapped the M state in wild-type bR, accumulated approximately 35% of this intermediate and solved the crystal structure (PDB ID: 1cwq and [45]). Both M state structures show quite similar changes on the proton release side of bR. The striking features of the extracellular domain are the conformational changes in the R82 and of the dyade E194/E204 in combination with displacements of water molecules. It seems that after proton release from the Schiff base towards D85 the effect of this movement of a positive charge results in a large downward reorientation of the positively charged R82 side chain to the negatively charged dyade E194/E204 which might directly or indirectly via a water molecule release the proton to the bulk medium. This switch function of R82 was predicted from theoretical considerations [70].

Both structural models do not provide a sufficiently clear picture of the proton pathway across the cytoplasmic domain. A common feature is the alterations in helices F and G which result in an enlargement of cavities thereby enabling the inward and outward diffusion of water molecules. However, a continuous water string below or above the position of D96 is not seen. Therefore the reprotonation of the Schiff base from D96 as

well as the reprotonation of this group is only possible by fluctuating water molecules and motions of amino acid side chains.

4. Proton transfer reactions

4.1. Vectorial proton transfer across bR

Proton translocation by bR is initiated by the light-induced isomerisation of the chromophore retinal. The structural motions of the retinal moiety set the scene for the following proton transfer reactions. The response of the apoprotein on retinal isomerisation is exemplified by an environmental change in the vicinity of the protonated residues D96 and D115. It can be deduced from the top spectrum in Fig. 5 that the C=O stretching vibration of these residues is altered and a band shift occurs as soon as in the L intermediate.

Isomerisation causes an electronic redistribution of retinal which leads to an increase in acidity of the retinal Schiff base (RSB) [71]. In addition, the Schiff base nitrogen is transferred into a less hydrogen-bonded environment [72] which destabilises the positive charge on the RSB and the high pK_a of the RSB ($pK_a^{(RSB)} = 13$ [73]) is decreased to approach the pK_a of D85. Consequently, the proton of the RSB is transferred to D85 and the M intermediate is established. This proton transfer reaction is monitored on the single vibrational level by FT-IR spectroscopy. The band at 1761 cm^{-1} in M (Fig. 5) has been assigned to the primary acceptor of the Schiff base proton, D85 [74]. The kinetics of this band are displayed on a logarithmic time scale (top trace in Fig. 6). The positive amplitude is due to the C=O vibration that appears when the aspartate at position 85 accepts the proton from the retinal Schiff base to form the corresponding aspartic acid (R-COOH) [75].

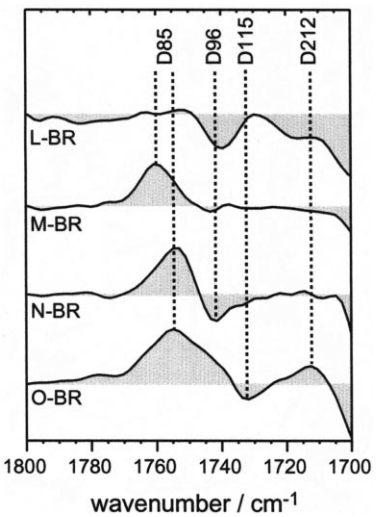

Fig. 5. Time-resolved FT-IR difference spectra of the photocycle intermediates L, M, N, and O in the carbonyl region. The band assignment (dashed vertical lines) illustrates the transient acid/base reactions of particular amino acids along with environmental changes in the vicinity of the respective carboxylic acid. Positive bands indicate the protonation of a carboxylate. Negative bands are due to the deprotonation of an acidic residue that is protonated in the ground-state bR.

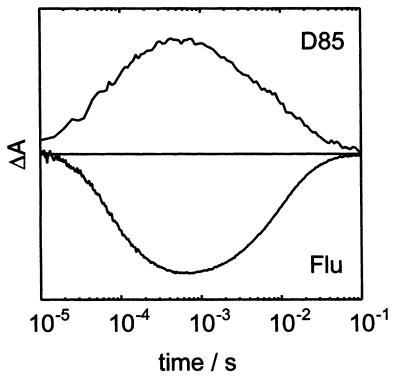

Fig. 6. Kinetics of the C=O stretching vibration of D85 at 1761 cm^{-1} (top trace) characteristic for the protonation and deprotonation reaction of D85. The bottom trace is the transient absorbance change at 489 nm of the surface-bound pH-indicator fluorescein (covalently linked to K129). The initial absorption decrease reflects light-induced proton release to the extracellular surface of bR ($\tau = 80$ μs). The subsequent transient absorption increase to the initial value ($\Delta A = 0$) is biphasic and indicates surface/bulk proton transfer (1 ms) and proton uptake by bR (15 ms), respectively. Both experiments have been performed at pH 7.2 and 20°C.

Concurrent with protonation of D85, a proton is released to the extracellular membrane surface with a time-constant of approximately 80 μs (bottom trace in Fig. 6). This reaction was probed by transient absorption spectroscopy in the visible wavelength range by using the pH-indicator fluo-

rescein selectively bound to the ε-amino group of K129 [76–80]. Two important consequences arise from the comparison of the two time traces in Fig. 6. First, the released proton must originate from another yet unidentified group since D85 stays protonated until the latest stage of the photocycle. Second, the protonation of D85 induces almost immediate proton release to the extracellular surface. The proton release reaction, however, is characterised by a lower activation energy (35–40 kJ/mol) than the deprotonation of the Schiff base (60–70 kJ/mol). This leads to the observation that at elevated temperatures proton release is much slower than proton transfer to D85 [78,81].

In several scenarios E194 and/or E204 have/has been proposed to be the terminal proton release group in the extracellular proton transfer cascade because of severe alterations in the proton release kinetics when one of these residues was exchanged [82–85]. However, difference bands due to E194 and E204 have not been detected in time-resolved FT-IR experiments [80,86]. The most apparent interpretation of this finding is the postulation of an hydrogen-bonded network in the extracellular channel [80] comprising D85, R82, the dyade of E194 and E204 as well as intervening water molecules. It must be stressed, however, that the proton release reaction leaves a deprotonated group within the protein and that this group has not been identified yet! Though the spatial position might favour E9 as the proton release group, time-resolved FT-IR and visible spectroscopy exclude E9 as well as E74 to be part of the proton release chain [86]. The functional role of water molecules in the proton release reaction was inferred from several studies [66,87–91] and direct evidence was provided by FT-IR spectroscopy [92–94].

R82 plays a critical role in proton release [95–98]. A combination of molecular dynamics, electrostatic and quantum chemical calculations suggested that R82 might flip from an 'upward' configuration with interaction to D85 to a 'downward' orientation [70,97] where it can interact with the E194/E204 dyade. This appealing mechanism readily explains how the information about the protonation state of D85 is transmitted to the proton release site and gives a reason for the fairly low activation energy of the proton release reaction (see above). Indeed, the transient rearrangement of the configuration of R82 is confirmed by the structural models of the M state [45,69].

Reprotonation of the RSB is accomplished by D96 [99–101]. The change in protonation state of D96 is detected in the N-bR difference spectrum by a negative band at 1741 cm^{-1} (Fig. 5) at which energy the C=O double bond vibrates [74,101]. The unusually high pK_a of 11.4 [102] drops by more than 4 pH-units to 7.1 [86] enabling D96 to reprotonate the RSB. This reaction defines the M-to-N transition. The increase in acidity of D96 might be caused by structural rearrangements observed with various techniques and discussed in the previous sections.

D96 itself is reprotonated from the cytoplasm. K41 and D38 are candidates for important residues lining the putative proton pathway from the cytoplasmic surface to D96. In fact, mutations of D38 exert drastic effects on the proton uptake reaction [103]. Unexpectedly, however, it is the reprotonation reaction of the RSB that is affected and not the reprotonation of D96. This puzzling result suggests an involvement of D38 in the conformational changes of the protein. Indeed, changes in tertiary structure during the photocycle are inhibited in the D38R mutant at neutral pH (see Section 3.2.4 and [67,103–105]). Mutations of K41, which is just one helix-turn further into the membrane (Fig. 2), did neither affect the kinetics of the photo- nor of the proton cycle (Heberle and Tittor, unpublished). Though spatial position and presumed charge favours the interaction with D38, K41 is dispensable for proton pumping.

In the final steps of proton translocation by bR, D85 dissociates. This reaction can be deduced as the slow component in the biphasic decay of the C=O stretch of D85 (top trace in Fig. 6). The fast component corresponds to a band shift from 1761 to 1755 cm^{-1} during the M decay [59,106]. However, the proton is not directly delivered to the proton release group but nearby D212 is protonated as an intermediate step (see bottom spectrum in Fig. 5 and [59,107]). With proton transfer

from D212 to the proton release group (XH) all proton donors and acceptors are reset to their initial states and the next sequence of proton transfer steps can be initiated by light.

It should be emphasised that the sequence of proton transfer reactions of bR has been described for neutral pH. Proton transfer reactions are intrinsically pH-dependent and bR is an excellent example for a manifold of pH-induced changes in kinetic and static properties (see [108] for a review).

4.2. Proton transfer reactions at the membrane surface

Proton pumping by bR leads to an acidification of the extracellular space. Using a highly water-soluble pH-indicator (pyranine), this reaction can be resolved in time and quanta. Proton release into the aqueous medium proceeds with a time constant of approximately 1 ms in an unbuffered solution. Proton uptake by bR is much slower ($\sim$ 15 ms) allowing to trace both reactions in an open system as purple membrane patches. Careful quantification of the transient response of the pH indicator by titration revealed a proton pumping stoichiometry of 1 H^+ per photoexcited bR [109]. Though quite controversial in the early days, most investigators now agree on this fact [4,78,81,110–112] and higher stoichiometries can be ruled out [113–116].

Covalently linking a pH indicator (fluorescein) to the membrane surface revealed, however, that proton release to the membrane surface of bR is much faster then proton release into the aqueous medium. Consequently, the protons released by bR dwell for approximately 1 ms along the surface of the purple membrane before they dissipate into the aqueous bulk phase. This surface/bulk proton transfer step is decoupled from the preceding internal proton transfer reactions and is a property of the interface between the membrane and the adjacent bulk water.

Proton transfer reactions along the membrane surface are of primary interest for chemiosmosis [117]. The debate about 'localised' and 'delocalised' proton movements [118] was revived to a certain extent [119–125] by experiments on PM patches at which pH-probes have been judiciously positioned [81,126]. This well-defined system allowed for a detailed analysis of the proton transfer along the membrane surface and into the aqueous bulk phase.

It turned out that a pH sensor bound to the cytoplasmic surface of a PM sheet responds much faster ($\tau = 230$ μs) to proton release ($\tau = 80$ μs, Fig. 6) than the sensor in the bulk water phase ($\tau = 1$ ms). The fast pH-equilibration of both membrane surfaces is surprising considering the large size of a PM patch (diameter of approx. 0.5 μm). But lateral proton transfer is not only fast, it is also efficient. Determination of the proton pumping stoichiometry revealed that the protons released by bR are quantitatively transferred to the opposite membrane surface.

Evidently, it is the long dwell time ($\sim$ 1 ms) along the membrane surface for protons to migrate distances that are in the range of proton generators and consumers [127]. The retarded surface-to-bulk proton transfer is not a peculiar property of PM. It is also observed in bR reconstituted in vesicles of various lipid composition [128] and in detergent micelles [129].

Besides protonatable groups [130], it is the structure and dynamics of surface water [131] that determines the surface/bulk proton transfer reaction. Specifically, it was shown by neutron scattering that the first hydration layer strongly interacts with the PM surface. A higher rotational mobility accompanied by a reduced translational motion of the surface water molecules is observed with respect to bulk water [132,133]. This might facilitate two-dimensional proton diffusion parallel to the membrane surface by a 'hop-and-turn' mechanism [134]. It can be assumed that upon freezing of the bulk water phase, the structural discontinuity between surface water and bulk water is eliminated. In fact, PM in ice does not exhibit the delayed surface/bulk proton transfer reaction [76].

The cytoplasmic surface of bR comprises many charged residues. Point mutations of several acidic amino acids (D36, D102, D104, E161) exerts a slight deceleration of proton uptake by bR [103]. The role of these amino acids was ascribed to efficiently collect protons from the aqueous bulk

phase and funnel them to the entrance of the cytoplasmic proton pathway where D38 is located. Time-resolved pH-jump experiments [135] and structural studies by electron crystallography [34] and atomic force microscopy [136] confirmed this proposal. Such a proton collecting antenna was also found in cytochrome *c* oxidase [137] which points to a general property of proton pumps.

5. Thermal equilibrium fluctuations 'lubricate' transitions of intermediates

The kinetics of the photocycle is determined by energy barriers which need to be surmounted during subsequent steps between the different intermediate states. In particular in the case of charge displacements and conformational changes, thermal equilibrium fluctuations provide a kind of 'stochastic driving force' to overcome these barriers. With respect to the microsecond and millisecond time regime, determining the transition rates between intermediates (with the exception of the early J and K intermediate), even faster picosecond fluctuations play a major role for the intermediate transitions. A powerful tool to study dynamical properties at this time scale, is given by the incoherent neutron scattering (INS). INS makes use of a large incoherent cross section of hydrogen nuclei (~ 40 times larger than the incoherent cross section of other elements), and is well suited to study all internal molecular motions in a time range from 10^{-10} to 10^{-14} s. With time-of-flight spectrometers the neutrons are measured as a function of energy transfer $\hbar\omega$ (related to the correlation time τ of the observed motion) and as a function of scattering angle (related to the momentum transfer $\boldsymbol{Q}$ of the neutron, giving information about the geometry of the motion [138–140]). Because the neutrons are scattered mainly at more or less homogeneously distributed hydrogens in the sample, the hydrogen nuclei serve as probes to monitor the 'overall fluctuations' of the investigated structures. A schematic representation of a time-of-flight spectrum is shown in Fig. 7. The quasielastic scattering, in general described by Lorentzians (parameterised by line widths H_n and amplitudes called quasielastic incoherent structure factors A_n), is related to stochastic motions or diffusion-like processes [see Eq. (1)]. Periodic vibrational motions (e.g. average 'mean square displacements' around a central position) are often faster and represented by vibrational peaks in the spectrum. All motions slower than τ_{res} ($1/\tau_{res} \sim$ resolution width Γ_{res}) contribute to the elastic peak. In the case of biological samples, where complex structures are related to a complex dynamical behaviour (and therefore a more complex spectrum as compared to Fig. 7), the inelastic scattering is often not easily distinguishable from the quasielastic scattering. With respect to an energy transfer range of a few meV, these spectra are characterised by more than only one quasielastic component. In measurements aiming to study dynamical properties of the biological macromolecules only (i.e. without solvent dynamics), the samples are hydrated with D_2O. In this case, all non-exchanged hydrogens are characterised by motions in restricted volumes (e.g. diffusion inside a sphere, but, for example, no long-range translational diffusion). The total scattering function S_{tot} includes not only the quasielastic incoherent structure factors A_n but also an elastic incoherent structure factor A_0 with

$$S_{tot}(\mathrm{Q},\omega) = \mathrm{e}^{-<\mathrm{u}^2>\mathrm{Q}^2} \cdot \left[A_0(\mathrm{Q}) \cdot \delta(\omega) + \sum_n A_n(\mathrm{Q}) \cdot L_n(H_n,\omega) \right], \quad (1)$$

where $\langle \mathrm{u}^2 \rangle$ gives the global average 'mean square displacements' of all vibrational motions (see for example [141–143]).

5.1. Temperature and hydration controls bR function via thermal equilibrium fluctuations

Environmental conditions, like temperature and the hydration level, have a distinct influence on the kinetics of the photocycle and on proton pumping [66,91,144]. On the other hand, the temperature and the amount of solvent molecules surrounding biological macromolecules strongly

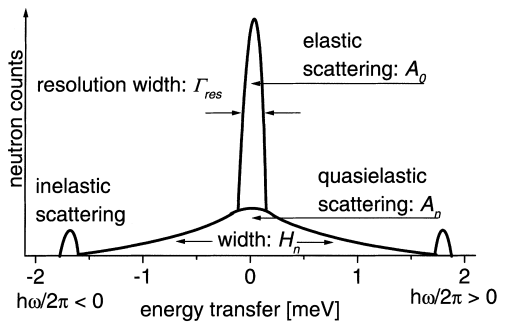

Fig. 7. Schematic representation of a neutron scattering spectrum.

determine dynamical properties [143]. The temperature dependence of picosecond equilibrium fluctuations have been measured with hydrated purple membranes ($h = 0.38$ g D_2O/g PM) and results of the analysis are presented in Fig. 8 [143]. As shown in Fig. 8b, a spectrum of purple membranes can be fitted with sufficient good quality by applying two quasielastic components included in the total scattering function. A narrow component (L_1) represents 'slow' and purely stochastic motions with an average correlation time of approximately 5.5 picoseconds (ps). A much broader component (L_2) is related to faster motions characterised by correlation times of approximately 0.5 ps. The temperature dependence of both quasielastic incoherent structure factors A_1 and A_2, shown in Fig. 8a, revealed a so-called 'dynamical transition' at a temperature T_d of approximately 190–220 K. Below T_d the slow fluctuations (A_1) are absent and for the fast motions A_2 (see inset of Fig. 8a) shows a linear T-dependence indicating a Debye–Waller behaviour typical for solid-like vibrational motions. The steep increase of A_1 (and of A_2) at T_d is characterised by an onset of stochastic 'large amplitude' motions (for some parts of the protein with amplitudes up to a few Å, see for example [142]) which are related to 'barrier crossing' between conformational substates [145]. Furthermore, A_1 exhibits an additional increase at approximately 260 K, which is related to the freezing point of the hydration water (T_{fh}). Depending on the initial hydration level (adjusted at room temperature) the hydration water is supercooled down to T_{fh} = 240–260 K before most of the solvent freezes (for more details see [146]). Since the equilibrium fluctuations are not only influenced by temperature but also by the hydration level, a reduced quasielastic incoherent structure factor is observed due to 'dehydration by cooling'. The

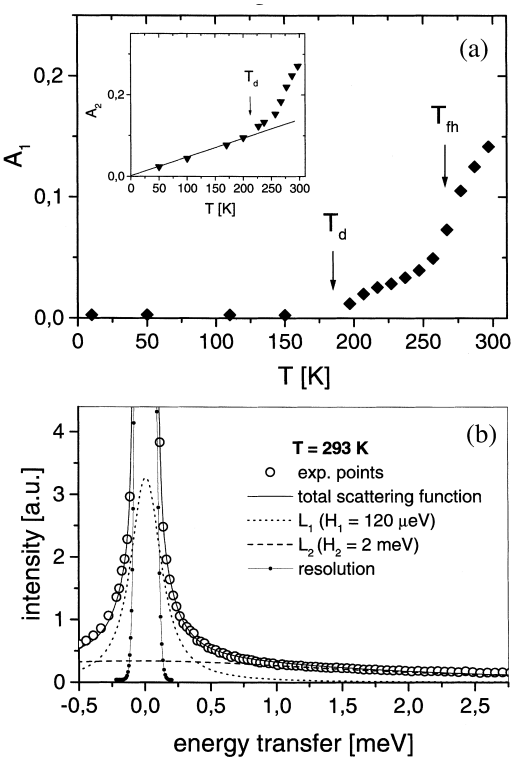

Fig. 8. The quasielastic incoherent structure factors A_1 (a) and A_2, given in the inset of (a), are shown as a function of temperature. Both structure factors exhibit a dynamical transition at T_d = 190–220 K. In (b) the fit of a typical spectrum as measured with hydrated purple membranes is shown. The spectrum was measured at the multichopper time-of-flight spectrometer NEAT located at the Hahn-Meitner-Institut, Berlin [140] using a wavelength of $\lambda = 5.1$ Å which corresponds to an elastic energy resolution of $\Gamma_{res} = 100$ μeV (FWHM). This spectrum was obtained by grouping all spectra measured in a range of scattering angles ϕ from 13.3° to 136.7° with a weighted mean of $\phi_{mean} = 55.4°$. The experimental points were fitted by the total scattering function composed of one elastic (resolution) and two quasielastic Lorentzian shaped contributions (L_1–L_2). The shape of the elastic scattering (resolution) was determined by vanadium measurements. This figure shows an enlargement of the quasielastic scattering, where the top of the frame corresponds to 10% of the elastic peak intensity.

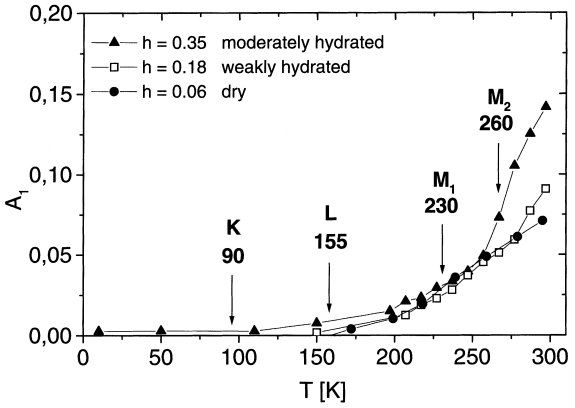

Fig. 9. Temperature dependence of the quasielastic incoherent structure factors A_1 of purple membrane samples with different hydration levels. For the intermediates K, L, M_1 and M_2 the dedicated trapping temperatures are referring to the corresponding value of A_1.

influence of temperature on the dynamical behaviour of samples at different initial hydration levels is shown in Fig. 9. In the low temperature regime up to a temperature of approximately 255 K the slow fluctuations (A_1) are rather similar for all hydration levels. Above this temperature A_1 is larger for higher hydration levels. The faster fluctuations (A_2) are less influenced by the hydration level (data not shown here, see [133,143]).

Regarding the temperature dependence of equilibrium fluctuations to particular temperatures where the individual intermediate states are trapped (as shown in Fig. 9) the following relation between photocycle kinetics and dynamical properties evolves: the first part of the photocycle (bR → J → K → L) seems not to be significantly influenced by large amplitude fluctuations. In contrast to this it appears, that the 'quantity' of large amplitude fluctuations is rate-limiting for transitions between the intermediates of the second half of the photocycle. The prominent tertiary structural change [62,63], which is supposed to occur during the $M_1 \rightarrow M_2$ transition, is inhibited below 230 K and at hydration levels below $h = 0.18$ [64]. Just between 230 K (M_1) and 260 K (M_2) a significant deviation in the 'quantity' of large amplitude fluctuations for different hydration levels is observed. Therefore, reduced large amplitude fluctuations seem to be responsible for prolonged or hindered transitions ($M_1 \rightarrow M_2$ and $M_2 \rightarrow N \rightarrow O \rightarrow bR$) [91] and disable tertiary structural changes at low temperatures and at low hydration levels [64]. The difference in the dynamical properties (see A_1 in Fig. 9) is largest above $T = 260$ K and decay rates of the M-intermediate (absorption changes measured at 412 nm, see [91]) are prolonged by one order of magnitude when lowering the hydration level from $h = 0.38$ to 0.18. This indicates that in particular the M-decay and the relaxation back to the ground state need a considerable 'quantity' of large amplitude picosecond fluctuations to 'lubricate' conformational relaxation of the protein scaffold on the millisecond time scale.

5.2. The role of lipids for structural flexibility and photocycle kinetics

The influence of lipids in the PM on the dynamical and functional properties of bR was investigated by comparing the natural purple membrane composed of 75% bR (w/w) and 25% lipid (w/w) and a delipidated PM having only 10% lipids (w/w) [91]. With both types of membranes measurements have been performed using moderately and weakly hydrated ($h = 0.38$ and $h = 0.18$, respectively) samples. The analysis of the INS measurements (performed only at room temperature) was somewhat different as compared to the phenomenological fitting procedure applied in the previous subsection. By considering the Q dependence of the scattering function and using specific models a more demonstrative interpretation of the data is possible. Based on the fact that re-orientational motions of polypeptide side groups represent a major part of motions in the picosecond time regime, an approximation of a 'free diffusion inside a sphere' was chosen (see [91]). In this model 'amplitudes' of motions are represented by the radius of the sphere r. With respect to an analysis of data within a limited energy transfer range (± 1 meV), only the slow fluctuations (with an average correlation time of approximately $\tau = 4.4$ ps related to a width of $H = 150$ μeV) were included in the fitting procedure. The sum of all incoherent structure factors is normalised to the unity (here only A_0 and A_1

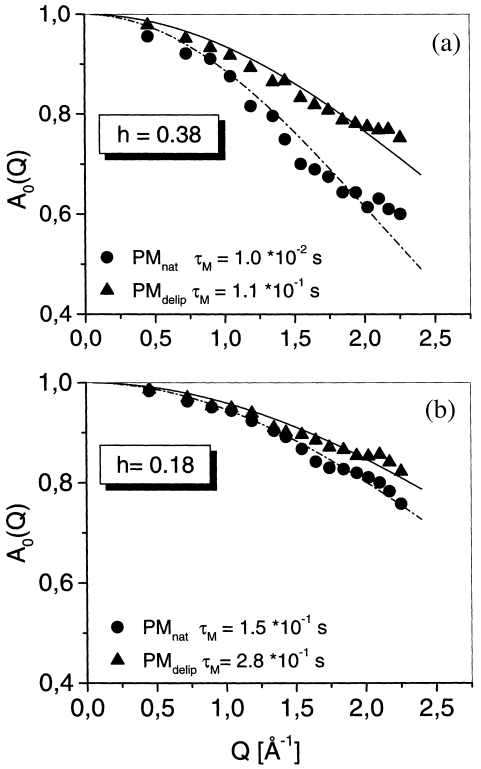

Fig. 10. Q-Dependence of elastic incoherent structure factors A_0 (solid symbols) as obtained at two different hydration levels for native and delipidated purple membranes. For PM_{nat} the modelfit (dashed–dotted line) revealed an 'amplitude' of motion $r = 0.77$ Å ($h = 0.38$) and $r = 0.52$ Å ($h = 0.18$). In the case of PM_{delip} (solid line) 'amplitudes' of $r = 0.57$ Å ($h = 0.38$) and $r = 0.45$ Å ($h = 0.18$) were obtained. For each sample the time constant τ_M for the M decay as determined from time-resolved absorption measurements at $\lambda = 412$ nm is given (for details see [91]).

with $A_0 + A_1 = 1$) and the decrease of A_0 with Q is a direct measure of the 'quantity' of internal flexibility of the sample. As shown in Fig. 10, the data have been analysed using this approach and revealed the following results: (i) a steeper decrease of the A_0 with Q for natural as compared to delipidated PM is related to larger 'amplitudes' r and therefore to a larger internal flexibility. The difference in flexibility between both types of membranes is relatively small in the case of weakly hydrated samples and more pronounced in the case of moderately hydrated samples. (ii) As already known from results given in the previous subsection, more complete hydration is related to increased internal flexibility. This effect is more pronounced in the case of natural PM samples as compared to delipidated PM samples.

The fact that the differences in the flexibility between natural and delipidated PM samples are much more pronounced in more complete hydrated samples, gives strong evidence that mainly the presence of hydration water, which is attached to the polar lipid head groups at high hydration levels [31,147], increases the internal flexibility of the protein–lipid complex [148]. The impressive accordance of the observed dynamical properties with the time constant τ_M characterising the M-decay (measured by time-resolved absorption changes, see [91]) given in Fig. 10 demonstrate, that restricted internal flexibility is related to prolonged M-decay. Therefore, one of the outstanding properties of lipids in the PM seems to be that mainly these lipids attract solvent molecules ensuring a sufficient structural flexibility of the whole PM, which is essential for a proper function of bR.

References

[1] D. Oesterhelt, W. Stoeckenius, Nat. New. Biol. 233 (1971) 149.
[2] D. Oesterhelt, W. Stoeckenius, Proc. Natl. Acad. Sci. USA 70 (1973) 2853.
[3] D. Oesterhelt, B. Hess, Eur. J. Biochem. 37 (1973) 316.
[4] R.H. Lozier, R.A. Bogomolni, W. Stoeckenius, Biophys. J. 15 (1975) 955.
[5] W. Stoeckenius, R.H. Lozier, W. Niederberger, Biophys. Struct. Mech. 3 (1977) 65.
[6] W. Sperling, P. Carl, C. Rafferty, N.A. Dencher, Biophys. Struct. Mech. 3 (1977) 79.
[7] J.K. Lanyi, G. Varo, Israel J. Chem. 35 (1995) 365.
[8] M.C. Nuss, W. Zinth, W. Kaiser, E. Koelling, D. Oesterhelt, Chem. Phys. Lett. 117 (1985) 1.
[9] R.A. Mathies, C.C. Brito, W.T. Pollard, C.V. Shank, Science 240 (1988) 777.
[10] G.H. Atkinson, D. Blanchard, H. Lemaire, T.L. Brack, H. Hayashi, Biophys. J. 55 (1989) 263.
[11] C.L. Hsieh, M.A. El-Sayed, M. Nicol, M. Nagumo, J.-H. Lee, Photochem. Photobiol. 38 (1983) 83.
[12] F. Siebert, W. Mäntele, Eur. J. Biochem. 130 (1983) 565.
[13] O. Weidlich, F. Siebert, Appl. Spectrosc. 47 (1993) 1394.
[14] J. Sasaki, A. Maeda, C. Kato, H. Hamaguchi, Biochemistry 32 (1993) 867.

[15] O. Weidlich, L. Ujj, F. Jager, G.H. Atkinson, Biophys. J. 72 (1997) 2329.
[16] A. Lewis, J. Spoonhower, R.A. Bogomolni, R.H. Lozier, W. Stoeckenius, Proc. Natl. Acad. Sci. USA 71 (1974) 4462.
[17] A.E. Blaurock, J. Mol. Biol. 93 (1975) 139.
[18] R. Henderson, P.N. Unwin, Biophys. Struct. Mech. 3 (1977) 121.
[19] P.N. Unwin, R. Henderson, J. Mol. Biol. 94 (1975) 425.
[20] R. Henderson, P.N. Unwin, Nature 257 (1975) 28.
[21] Y.A. Ovchinnikov, N.G. Abdulaev, M.Y. Feigina, A.V. Kiselev, N.A. Lobanov, FEBS Lett. 100 (1979) 219.
[22] D.M. Engelman, R. Henderson, A.D. McLachlan, B.A. Wallace, Proc. Natl. Acad. Sci. USA 77 (1980) 2023.
[23] D.M. Engelman, G. Zaccai, Proc. Natl. Acad. Sci. USA 77 (1980) 5894.
[24] J. Trewhella, S. Anderson, R. Fox et al., Biophys. J. 42 (1983) 233.
[25] J. Trewhella, J.L. Popot, G. Zaccai, D.M. Engelman, EMBO J. 5 (1986) 3045.
[26] J.L. Popot, D.M. Engelman, O. Gurel, G. Zaccai, J. Mol. Biol. 210 (1989) 829.
[27] J.S. Jubb, D.L. Worcester, H.L. Crespi, G. Zaccai, EMBO J. 3 (1984) 1455.
[28] F. Seiff, I. Wallat, P. Ermann, M.P. Heyn, Proc. Natl. Acad. Sci. USA 82 (1985) 3227.
[29] T. Hauss, S. Grzesiek, H. Otto, J. Westerhausen, M.P. Heyn, Biochemistry 29 (1990) 4904.
[30] G. Büldt, K. Konno, K. Nakanishi, H.J. Plöhn, B.N. Rao, N.A. Dencher, Photochem. Photobiol. 54 (1991) 873.
[31] G. Papadopoulos, N.A. Dencher, G. Zaccai, G. Büldt, J. Mol. Biol. 214 (1990) 15.
[32] R. Henderson, J.M. Baldwin, T.A. Ceska, F. Zemlin, E. Beckmann, K.H. Downing, J. Mol. Biol. 213 (1990) 899.
[33] N. Grigorieff, T.A. Ceska, K.H. Downing, J.M. Baldwin, R. Henderson, J. Mol. Biol. 259 (1996) 393.
[34] Y. Kimura, D.G. Vassylyev, A. Miyazawa et al., Nature 389 (1997) 206.
[35] K. Mitsuoka, T. Hirai, K. Murata et al., J. Mol. Biol. 286 (1999) 861.
[36] H. Michel, D. Oesterhelt, Proc. Natl. Acad. Sci. USA 77 (1980) 1283.
[37] G.F. Schertler, H.D. Bartunik, H. Michel, D. Oesterhelt, J. Mol. Biol. 234 (1993) 156.
[38] E.M. Landau, J.P. Rosenbusch, Proc. Natl. Acad. Sci. USA 93 (1996) 14532.
[39] E. Pebay-Peyroula, G. Rummel, J.P. Rosenbusch, E.M. Landau, Science 277 (1997) 1676.
[40] J. Heberle, G. Büldt, E. Koglin, J.P. Rosenbusch, E.M. Landau, J. Mol. Biol. 281 (1998) 587.
[41] H. Luecke, H.T. Richter, J.K. Lanyi, Science 280 (1998) 1934.
[42] H. Luecke, B. Schobert, H.T. Richter, J.P. Cartailler, J.K. Lanyi, J. Mol. Biol. 291 (1999) 899.
[43] L. Essen, R. Siegert, W.D. Lehmann, D. Oesterhelt, Proc. Natl. Acad. Sci. USA 95 (1998) 11673.
[44] K. Takeda, H. Sato, T. Hino et al., J. Mol. Biol. 283 (1998) 463.
[45] H.J. Sass, J. Berendzen, D. Neff, R. Gessenich, P. Ormos, G. Büldt (1999) [submitted].
[46] T. Althaus, W. Eisfeld, R. Lohrmann, M. Stockburger, Israel J. Chem. 35 (1995) 227.
[47] R.A. Mathies, S.W. Lin, J.B. Ames, W.T. Pollard, Annu. Rev. Biophys. Biophys. Chem. 20 (1991) 491.
[48] W. Mäntele, Trends Biochem. Sci. 18 (1993) 197.
[49] W. Uhmann, A. Becker, C. Taran, F. Siebert, Appl. Spectrosc. 45 (1991) 390.
[50] R. Rammelsberg, B. Heßling, H. Chorongiewski, K. Gerwert, Appl. Spectrosc. 51 (1997) 558.
[51] X. Hu, H. Frei, T.G. Spiro, Biochemistry 35 (1996) 13001.
[52] K.J. Rothschild, J. Bioenerg. Biomembr. 24 (1992) 147.
[53] K. Gerwert, Biochim. Biophys. Acta 1101 (1992) 147.
[54] A. Maeda, Israel J. Chem. 35 (1995) 387.
[55] F. Siebert, Methods Enzymol. 246 (1995) 501.
[56] J. Heberle, Biochim. Biophys. Acta (2000) [in press].
[57] J. Heberle, C. Zscherp, Appl. Spectrosc. 50 (1996) 588.
[58] J. Heberle, Recent Res. Dev. Appl. Spectrosc. 2 (1999) 147.
[59] C. Zscherp, J. Heberle, J. Phys. Chem. B 101 (1997) 10542.
[60] S.O. Smith, J.A. Pardoen, P.P. Mulder, B. Curry, J. Lugtenburg, R.A. Mathies, Biochemistry 22 (1983) 6141.
[61] R.M. Glaeser, J. Baldwin, T.A. Ceska, R. Henderson, Biophys. J. 50 (1986) 913.
[62] N.A. Dencher, D. Dresselhaus, G. Zaccai, G. Büldt, Proc. Natl. Acad. Sci. USA 86 (1989) 7876.
[63] M.H.J. Koch, N.A. Dencher, D. Oesterhelt, H.J. Plöhn, G. Rapp, G. Büldt, EMBO J. 10 (1991) 521.
[64] H.J. Sass, I.W. Schachowa, G. Rapp et al., EMBO J. 16 (1997) 1484.
[65] G. Varo, J.K. Lanyi, Biochemistry 29 (1990) 2241.
[66] G. Thiedemann, J. Heberle, N.A. Dencher, in: J.L. Rigaud (Ed.), Structures and Functions of Retinal Proteins, John Libbey Eurotext Ltd, 1992, p. 217.
[67] H.J. Sass, R. Gessenich, M.H. Koch et al., Biophys. J. 75 (1998) 399.
[68] K. Edman, P. Nollert, A. Royant et al., Nature 401 (1999) 822.
[69] H. Luecke, B. Schobert, H.T. Richter, J.P. Cartailler, J.K. Lanyi, Science 286 (1999) 255.
[70] C. Scharnagl, S.F. Fischer, Chem. Phys. 212 (1996) 231.
[71] K. Schulten, P. Tavan, Nature 272 (1978) 85.
[72] L.S. Brown, Y. Gat, M. Sheves et al., Biochemistry 33 (1994) 12001.
[73] S. Druckmann, M. Ottolenghi, A. Pande, J. Pande, R.H. Callender, Biochemistry 21 (1982) 4953.
[74] M.S. Braiman, T. Mogi, T. Marti, L.J. Stern, H.G. Khorana, K.J. Rothschild, Biochemistry 27 (1988) 8516.
[75] K. Fahmy, O. Weidlich, M. Engelhard, J. Tittor, D. Oesterhelt, F. Siebert, Photochem. Photobiol. 56 (1992) 1073.
[76] J. Heberle, N.A. Dencher, FEBS Lett. 277 (1990) 277.

[77] N.A. Dencher, J. Heberle, C. Bark et al., Photochem. Photobiol. 54 (1991) 881.
[78] J. Heberle, N.A. Dencher, Proc. Natl. Acad. Sci. USA 89 (1992) 5996.
[79] Y. Cao, L.S. Brown, J. Sasaki, A. Maeda, R. Needleman, J.K. Lanyi, Biophys. J. 68 (1995) 1518.
[80] R. Rammelsberg, G. Huhn, M. Lübben, K. Gerwert, Biochemistry 37 (1998) 5001.
[81] J. Heberle, J. Riesle, G. Thiedemann, D. Oesterhelt, N.A. Dencher, Nature 370 (1994) 379.
[82] L.S. Brown, J. Sasaki, H. Kandori, A. Maeda, R. Needleman, J.K. Lanyi, J. Biol. Chem. 270 (1995) 27122.
[83] S.P. Balashov, E.S. Imasheva, T.G. Ebrey, N. Chen, D.R. Menick, R.K. Crouch, Biochemistry 36 (1997) 8671.
[84] A.K. Dioumaev, H.T. Richter, L.S. Brown et al., Biochemistry 37 (1998) 2496.
[85] J.K. Lanyi, J. Biol. Chem. 272 (1997) 31209.
[86] C. Zscherp, R. Schlesinger, J. Tittor, D. Oesterhelt, J. Heberle, Proc. Natl. Acad. Sci. USA 96 (1999) 5498.
[87] P. Hildebrandt, M. Stockburger, Biochemistry 23 (1984) 5548.
[88] R. Korenstein, B. Hess, Nature 270 (1977) 184.
[89] G. Varo, L. Keszthelyi, Biophys. J. 47 (1985) 243.
[90] G. Varo, J.K. Lanyi, Biophys. J. 59 (1991) 313.
[91] J. Fitter, S.A. Verclas, R.E. Lechner, H. Seelert, N.A. Dencher, FEBS Lett. 433 (1998) 321.
[92] A. Maeda, J. Sasaki, Y. Shichida, T. Yoshizawa, Biochemistry 31 (1992) 462.
[93] A. Maeda, J. Sasaki, Y. Yamazaki, R. Needleman, J.K. Lanyi, Biochemistry 33 (1994) 1713.
[94] W.B. Fischer, S. Sonar, T. Marti, H.G. Khorana, K.J. Rothschild, Biochemistry 33 (1994) 12757.
[95] R. Govindjee, S. Misra, S.P. Balashov, T.G. Ebrey, R.K. Crouch, D.R. Menick, Biophys. J. 71 (1996) 1011.
[96] S.P. Balashov, R. Govindjee, M. Kono et al., Biochemistry 32 (1993) 10331.
[97] C. Scharnagl, J. Hettenkofer, S.F. Fischer, J. Phys. Chem. 99 (1995) 7787.
[98] A. Kusnetzow, D.L. Singh, C.H. Martin, I.J. Barani, R.R. Birge, Biophys. J. 76 (1999) 2370.
[99] H. Otto, T. Marti, M. Holz et al., Proc. Natl. Acad. Sci. USA 86 (1989) 9228.
[100] H.J. Butt, K. Fendler, E. Bamberg, J. Tittor, D. Oesterhelt, EMBO J. 8 (1989) 1657.
[101] K. Gerwert, B. Hess, J. Soppa, D. Oesterhelt, Proc. Natl. Acad. Sci. USA 86 (1989) 4943.
[102] S. Száraz, D. Oesterhelt, P. Ormos, Biophys. J. 67 (1994) 1706.
[103] J. Riesle, D. Oesterhelt, N.A. Dencher, J. Heberle, Biochemistry 35 (1996) 6635.
[104] T. Rink, J. Riesle, D. Oesterhelt, K. Gerwert, H.J. Steinhoff, Biophys. J. 73 (1997) 983.
[105] S. Subramaniam, I. Lindahl, P. Bullough et al., J. Mol. Biol. 287 (1999) 145.
[106] K. Gerwert, G. Souvignier, B. Hess, Proc. Natl. Acad. Sci. USA 87 (1990) 9774.
[107] A.K. Dioumaev, L.S. Brown, R. Needleman, J.K. Lanyi, Biochemistry 38 (1999) 10070.
[108] T.G. Ebrey, in: M. Jackson (Ed.), Thermodynamics of Membranes, Receptors and Channels, CRC Press, Inc, Boca Raton FL, 1993, p. 353.
[109] S. Grzesiek, N.A. Dencher, Proc. Natl. Acad. Sci. USA 85 (1988) 9509.
[110] R.H. Lozier, W. Niederberger, R.A. Bogomolni, S. Hwang, W. Stoeckenius, Biochim. Biophys. Acta 440 (1976) 545.
[111] L.A. Drachev, A.D. Kaulen, V.P. Skulachev, FEBS Lett. 209 (1986) 316.
[112] G. Varo, J.K. Lanyi, Biochemistry 29 (1990) 6858.
[113] D.R. Ort, W.W. Parson, Biophys. J. 25 (1979) 341.
[114] R. Govindjee, T.G. Ebrey, A.R. Crofts, Biophys. J. 30 (1980) 231.
[115] D. Kuschmitz, B. Hess, Biochemistry 20 (1981) 5950.
[116] L. Stryer, Biochemistry, W.H. Freeman & Company, 1995.
[117] P. Mitchell, Nature 191 (1961) 144.
[118] D.G. Nicholls, S.J. Ferguson, Bioenergetics 2, Academic Press Inc, San Diego, 1992.
[119] S.J. Ferguson, Curr. Biol. 5 (1995) 25.
[120] P. Scherrer, Nature 374 (1995) 222.
[121] J. Teissié, Nature 379 (1996) 305.
[122] B. Gabriel, J. Teissié, Proc. Natl. Acad. Sci. USA 93 (1996) 14521.
[123] E. Nachliel, M. Gutman, S. Kiryati, N.A. Dencher, Proc. Natl. Acad. Sci. USA 93 (1996) 10747.
[124] Y.N. Antonenko, P. Pohl, FEBS Lett. 429 (1998) 197.
[125] I.P. Krasinskaya, M.V. Lapin, L.S. Yaguzhinsky, FEBS Lett. 440 (1998) 223.
[126] U. Alexiev, R. Mollaaghababa, P. Scherrer, H.G. Khorana, M.P. Heyn, Proc. Natl. Acad. Sci. USA 92 (1995) 372.
[127] J. Heberle, N.A. Dencher, in: J.L. Rigaud (Ed.), Structures and Functions of Retinal Proteins, John Libbey Eurotext Ltd, 1992, p. 221.
[128] J. Heberle, N.A. Dencher, in: T. Bountis (Ed.), Proton Transfer in Hydrogen-Bonded Systems, Plenum Press, New York, 1992, p. 187.
[129] P. Scherrer, U. Alexiev, T. Marti, H.G. Khorana, M.P. Heyn, Biochemistry 33 (1994) 13684.
[130] E. Nachliel, M. Gutman, FEBS Lett. 393 (1996) 221.
[131] E. Westhof, Water and Biological Macromolecules, CRC Press, Boca Raton, FL, 1993.
[132] R.E. Lechner, N.A. Dencher, J. Fitter, G. Büldt, A.V. Belushkin, Biophys. Chem. 49 (1994) 91.
[133] J. Fitter, R.E. Lechner, N.A. Dencher, J. Phys. Chem. B 103 (1999) 8036.
[134] J.F. Nagle, S. Tristram-Nagle, J. Membr. Biol. 74 (1983) 1.
[135] S. Checover, E. Nachliel, N.A. Dencher, M. Gutman, Biochemistry 36 (1997) 13919.
[136] D.J. Müller, H.J. Sass, S.A. Müller, G. Büldt, A. Engel, J. Mol. Biol. 285 (1999) 1903.

[137] Y. Marantz, E. Nachliel, A. Aagaard, P. Brzezinski, M. Gutman, Proc. Natl. Acad. Sci. USA 95 (1998) 8590.
[138] R.E. Lechner, in: F. Beniere, C.R.A. Catlow (Eds.), Mass Transport in Solids, Plenum Publ. Corp, New York, 1983, p. 169.
[139] M. Bee, Quasi-Elastic Neutron Scattering, Adam & Hilger, Philadelphia, 1988.
[140] R.E. Lechner, R. Melzer, J. Fitter, Physica B 226 (1996) 86.
[141] W. Doster, S. Cusack, W. Petry, Nature 337 (1989) 754.
[142] J. Fitter, R.E. Lechner, G. Büldt, N.A. Dencher, Proc. Natl. Acad. Sci. USA 93 (1996) 7600.
[143] J. Fitter, R.E. Lechner, N.A. Dencher, Biophys. J. 73 (1997) 2126.
[144] T. Iwasa, F. Tokunaga, T. Yoshizawa, Biophys. Struct. Mech. 6 (1980) 253.
[145] H. Frauenfelder, G.A. Petsko, D. Tsernoglou, Nature 280 (1979) 558.
[146] R.E. Lechner, J. Fitter, N.A. Dencher, T. Hauss, J. Mol. Biol. 277 (1998) 593.
[147] P.K. Rogan, G. Zaccai, J. Mol. Biol. 145 (1981) 281.
[148] J. Fitter, R.E. Lechner, N.A. Dencher, in: S. Cusack, M. Büttner, M. Ferrand (Eds.), Biological Macromolecular Dynamics, Adenine Press, Schenectady, NY, 1997, p. 123.